4. Slow Uniform Growth and Spatial Frequency-Doubling

In this chapter we investigate the patterning properties of the reaction-diffusion mechanism on a slow uniformly growing domain in one spatial dimension. In particular we are interested in how the behaviour of the solution depends on the new timescale that is introduced into the equation as a result of domain growth, and how this timescale interacts with the timescale for pattern formation in the static reaction-diffusion problem.

Spatial frequency-doubling has been reported by several authors [3, 64, 107]. The phenomenon consists of regular doubling of the spatial frequency of the standing wave pattern on the unit interval. On the dimensional domain this behaviour corresponds to regular doubling of the mode of spatial pattern. The period for frequency-doubling (hereafter FD) will be shown to be the time taken for the dimensional domain to double in length. In this chapter we examine this behaviour in detail, suggesting a symmetry of the governing equation which may underly the patterning behaviour, and we investigate dependence on parameters and the functional form describing the growth.

4.1 Slow and Fast Dynamics

The evolution equations describing reaction and diffusion in one spatial dimension[1] for two interacting species with concentrations $u(x,t)$ and $v(x,t)$, with uniform domain growth may be written as

$$u_t = \frac{1}{\gamma}u_{xx} + f(u,v) - \rho\sigma(t)u \tag{4.1}$$

$$v_t = \frac{d}{\gamma}v_{xx} + g(u,v) - \rho\sigma(t)v \tag{4.2}$$

$$\gamma_t = 2\rho\gamma_0\sigma(t)\exp\left[2\rho\int_0^t \sigma\left(\bar{t}\right)\mathrm{d}\bar{t}\right] \tag{4.3}$$

where v is the self-activator, which is defined on

$$x \in [0,1]\,, \quad t \in [0,\infty)\,. \tag{4.4}$$

We impose zero-flux boundary conditions

$$u_x = v_x = 0 \quad \text{on} \quad x = 0, 1. \tag{4.5}$$

[1] For convenience we adopt the notation x for the uniformly scaled position, such that $x \in [0,1]$.

Initial conditions are random perturbations about the homogeneous steady state of the kinetics, (u_s, v_s) where

$$f(u_s, v_s) - \rho\sigma(0)u_s = 0 \tag{4.6}$$

$$g(u_s, v_s) - \rho\sigma(0)v_s = 0. \tag{4.7}$$

For slow growth we have

$$0 < \rho \ll 1 \tag{4.8}$$

such that the growth timescale $1/\rho \gg 1$, and we recall that pattern formation is on an $\mathcal{O}(1)$ timescale. The separation of scales that this produces gives two regimes, with evolution on a slow and a fast timescale respectively. If we introduce a slow time variable, $\tau = \rho t$, then asymptotically as $\rho \to 0$ we have the slow subsystem (when $u_\tau, v_\tau \ll \mathcal{O}(1/\rho)$):

$$u_{xx} = -\gamma f \tag{4.9}$$

$$dv_{xx} = -\gamma g \tag{4.10}$$

$$\gamma_\tau = \gamma_0 \exp\left[2\rho \int_0^{\tau/\rho} \sigma\left(\bar{t}\right) \mathrm{d}\bar{t}\right] \tag{4.11}$$

for which the quasi-steady solutions are parameterised by γ. This adiabatic limit holds except where $u_\tau, v_\tau \sim \mathcal{O}(1/\rho)$ for which we have the fast system

$$u_t = \frac{1}{\gamma} u_{xx} + f \tag{4.12}$$

$$v_t = d\frac{1}{\gamma} v_{xx} + g \tag{4.13}$$

where γ is constant. The fast subsystem governs the reorganisation of patterns away from the quasi-steady regime. The extra terms in the kinetics (the dilution terms) are $\mathcal{O}(\rho)$ and so do not feature to leading order.

This scaling arises very naturally in the equations and for zero-flux boundary conditions may be verified by considering the function

$$\phi(\tau;\rho) \equiv \frac{\mathrm{d}}{\mathrm{d}\tau} \int_0^1 \left[u(x,\tau;\rho) + v(x,\tau;\rho)\right] \mathrm{d}x \tag{4.14}$$

$$= \frac{1}{\rho} \int_0^1 \left[f(u,v) + g(u,v)\right] \mathrm{d}x \tag{4.15}$$

which should stay close to zero during slow dynamics, and scale as $1/\rho$ in the fast dynamic regime. Numerically we find that $\phi(\tau;\rho)$ remains close to zero in the quasi-steady state and has a maximum during the reorganisation of pattern (reaching the same maximal value independent of the particular pattern mode) where

$$\phi_{max} = \max_{\tau \in [0,\infty)} \left(\phi\left(\tau;\rho\right)\right) \sim \frac{1}{\rho}. \tag{4.16}$$

We will present concrete examples below.

Thus for the slow growth limit, $\rho \ll 1$, the analysis suggests periods of quasi-steady behaviour interspersed with fast transitions corresponding to fast dynamical reorganisation to a different pattern. This does not tell us anything about which pattern modes are expected in the sequence, or whether the sequence of patterns is sensitive to initial conditions.

Heuristically we may describe the process of generation of a pattern sequence in the model, under these two timescales, as follows. The initial bifurcation from the homogeneous steady state is through a diffusion-driven instability near the critical point $\gamma = \gamma_c$ which may be derived from linear stability theory. Linear growth of the destabilising mode and subsequent saturation to a large amplitude pattern ensues. The pattern then evolves in two dynamical regimes. The amplitude of the pattern is gently modulated in the quasi-steady state as γ changes with time. A pattern persists until at some point the solution undergoes a transition to a new quasi-steady pattern; undergoing a fast dynamic reorganisation (activator peak *splitting* and separation for Schnakenberg kinetics). Subsequently a pattern of higher spatial frequency (for γ increasing) is established which in turn persists, with slow amplitude modulation, before the solution undergoes further transitions.

4.2 Spatial Frequency-Doubling for Exponential Domain Growth

Growth at a constant strain rate, $S(t) = \rho\sigma(t) = \rho$, corresponds to an exponential uniform domain growth

$$\Gamma(X,t) = X\exp(\rho t). \tag{4.17}$$

Under this growth, FD is observed within a parameter regime that is to be determined. We illustrate this with a concrete example using the Schnakenberg scheme for the nonlinear kinetics (see Appendix A.1)

$$f(u,v) = b - uv^2 \tag{4.18}$$

$$g(u,v) = a + uv^2 - v \tag{4.19}$$

where $g(u,v)$ is the kinetic function for the self-activating species v and $f(u,v)$ is the inhibitor kinetics.

Numerical Solution. We have computed numerical solutions of equation (4.1)–(4.3) with Schnakenberg kinetics, zero-flux boundary conditions (4.4) and exponential growth function (4.17) using a finite differences scheme which uses the method of lines for spatial discretisation and Gear's method for integration in time, as implemented in the NAG numerical routine `D03PCF`. The kinetic parameters here and in all other simulations with Schnakenberg kinetics are $a = 0.1$, $b = 0.9$ and we take the ratio of diffusivities $d = 0.01$, unless described otherwise. The initial conditions in each case are random fluctuations about the kinetic steady state concentrations, with a uniform distribution and maximum deviation of 0.5%. Typically we take 1001 spatial points in $[0,1]$, however, in all simulations we have at least 10 spatial points per wavelength

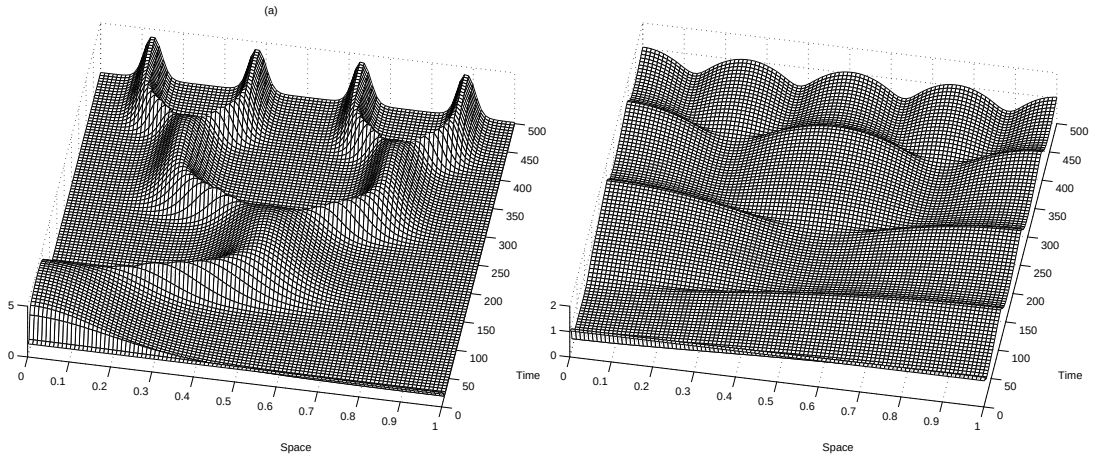

FIGURE 4.1 The spatial frequency-doubling sequence of patterns on an exponentially growing domain. We plot the evolution of (a) activator $v(x,t)$ and (b) inhibitor $u(x,t)$ concentrations for Schnakenberg kinetics, with $d = 0.01$ and $\rho = 0.005$. Pattern transitions are by activator peak splitting. The inhibitor profile is in spatial antiphase with the activator solution (the kinetics are of cross type). The accuracy in the time integration is 1.0×10^{-6}.

of pattern. Typical solutions are shown in Figure 4.1 for (a) activator and (b) inhibitor, and in Figure 4.2 the solution profile for the activator species is plotted on the dimensional growing domain.

In Figure 4.3(a) we plot the evolution of the maximum amplitude for each species (activator and inhibitor) given by

$$\eta_i(t) = \max_{x\in[0,1]} \left(c_i(x,t)\right), \quad i = 1,2 \tag{4.20}$$

which illustrates the periodic nature of the pattern sequence. The pattern changes at intervals corresponding to the time taken for the domain to double in length, which gives the period $\Delta t = (\ln 2)/\rho$, where $\Delta t \approx 693$ for the parameters in the simulation. Adding the equations for u and v written in the slow time variable $\tau = \rho t$ and integrating over the domain, we find

$$\phi(\tau) \equiv \frac{\mathrm{d}}{\mathrm{d}\tau}\int_0^1 (u+v)\,\mathrm{d}x = \frac{1}{\rho}\left[(a+b) - \int_0^1 v\,\mathrm{d}x\right], \tag{4.21}$$

where in the quasi-steady state $\phi \approx 0$, shown in Figure 4.3(b). Here ϕ is plotted against t for ease of comparison with previous figures. The evolution of ϕ illustrates the two dynamic regimes, with ϕ remaining close to zero except during the transition between quasi-steady patterns. The dependence on the strain rate ρ of the maximum value, ϕ_{max}, is presented in Figure 4.4.

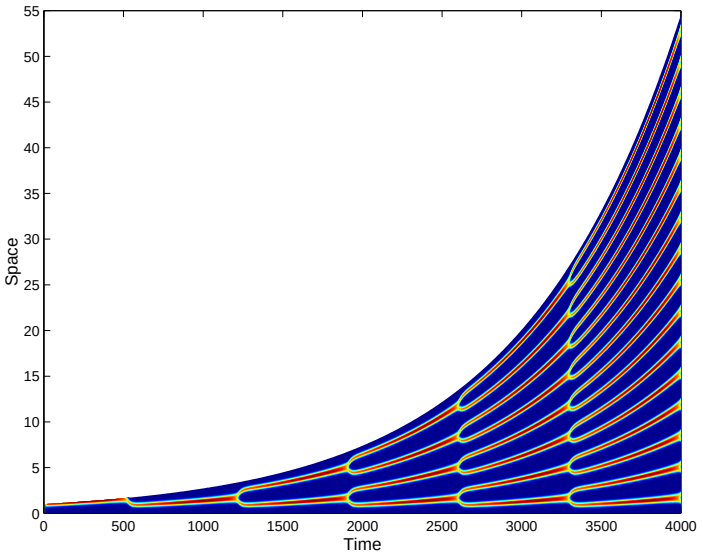

FIGURE 4.2 Spatial frequency-doubling on the dimensional domain—evolution of the activator $v(x,t)$ plotted on the exponentially growing domain showing periodic transitions as the domain length doubles. Kinetic parameters for the Schnakenberg scheme are as in Figure 4.1, with $\rho = 0.001$. Shading is from blue at zero concentration to red at high concentration ($v = 5$).

4.2.1 Symmetry Analysis. Frequency-doubling corresponds to a sequence in which the spatial frequency of the pattern regularly doubles, and no other pattern modes enter the sequence. Self-similarity of pattern modes can be used to predict necessary conditions under which this sequence is expected in our model. As $\gamma(t)$ is a monotonically increasing function we can eliminate t from the evolution equations (4.1) and (4.2) in favour of γ to give (for each species)

$$h(\gamma)\frac{\partial c}{\partial \gamma} = \frac{d}{\gamma}\frac{\partial^2 c}{\partial x^2} + R(c) - \frac{h(\gamma)}{2\gamma}c \tag{4.22}$$

where $h(\gamma) \equiv \mathrm{d}\gamma/\mathrm{d}t$, and for the final (dilution) term we have used $\mathrm{d}\gamma/\mathrm{d}t = 2\rho\sigma(t)\gamma(t)$. Let us assume that at $\gamma = \gamma^*$ the solution has spatial profile $c(x,\gamma^*)$. At any point in the sequence, in particular at $\gamma = \gamma^*$, a pattern of twice the spatial frequency $q_2(x,\gamma)$ may be constructed by applying the tent map $p_2(x)$ given in section 2.4.3, where

$$q_2(x,\gamma') \equiv c(p_2(x),\gamma'). \tag{4.23}$$

The transformed quantity q_2 in turn satisfies the evolution equation

$$h(\gamma')\frac{\partial q_2}{\partial \gamma'} = \frac{d}{4\gamma'}\frac{\partial^2 q_2}{\partial x^2} + R(q_2) - \frac{h(\gamma')}{2\gamma'}q_2. \tag{4.24}$$

Also, considering equation (4.22) we can see that the quantity $c(x,4\gamma')$ must satisfy the equation

$$\frac{1}{4}h(4\gamma')\frac{\partial c}{\partial \gamma'} = \frac{d}{4\gamma'}\frac{\partial^2 c}{\partial x^2} + R(c) - \frac{h(4\gamma')}{8\gamma'}c. \tag{4.25}$$

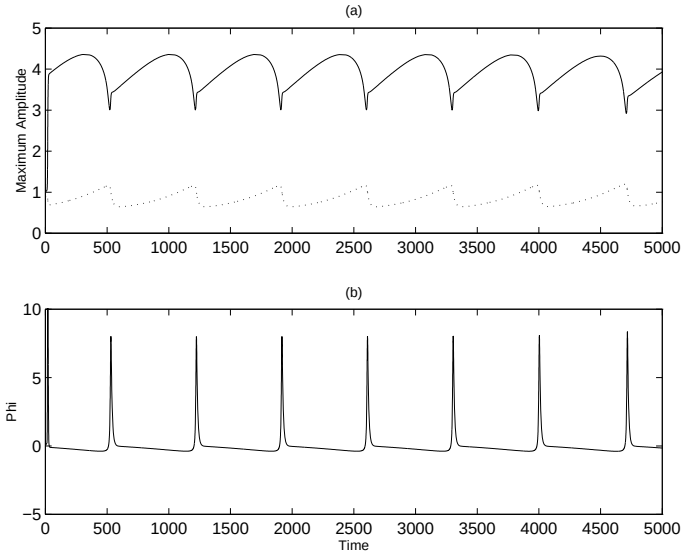

FIGURE 4.3 Periodicity in the transitions between quasi-steady patterns for exponential domain growth. We plot the evolution of (a) the maximum pattern amplitude for activator $\eta_2(t)$ (solid line) and inhibitor $\eta_1(t)$ (dotted line) species and (b) $\phi(t)$ (as defined in equation (4.21), here plotted against the fast time variable $t = \tau/\rho$ for ease of comparison), with parameters for the Schnakenberg kinetics as in Figure 4.1, and exponential domain growth with $\rho = 0.001$.

Now $c(x, 4\gamma')$ and $q_2(x, \gamma')$ satisfy the same equation if

$$h(4\gamma') = 4h(\gamma') \tag{4.26}$$

so that the left hand sides are the same and the final terms from the right hand side of the equations also match. Recalling that $h(\gamma) = \mathrm{d}\gamma/\mathrm{d}t$, this demands that the time dependence of γ, and hence the domain growth, is exponential,

$$\gamma(t) \propto \exp(2\rho t), \quad r(t) = \exp(\rho t) \tag{4.27}$$

so that the strain rate is constant in time. Furthermore, if at $\gamma = \gamma^*$ we find that in fact

$$q_2(x, \gamma^*) = c(x, 4\gamma^*), \quad \forall x \in [0, 1], \tag{4.28}$$

the *matching condition*, then the profiles are equivalent and, assuming uniqueness of solutions to the evolution equation for given initial and boundary conditions, they will continue to coincide for all time such that $\gamma > \gamma^*$. We have made no assumptions about γ^* or the spatial profile at γ^*: this observation holds in both quasi-steady and fast (transition) dynamical regimes.

We have shown that under exponential growth the quantities $q_2(x, \gamma) \equiv c(p_2(x), \gamma)$ and $c(x, 4\gamma)$ satisfy the same evolution equation. Below we investigate the consequences for FD. From the spatial profile $c(x, \gamma^*)$ we can construct $q_2(x, \gamma^*) \equiv c(p_2(x), \gamma^*)$ which by definition has twice the spatial frequency. Let us suppose that

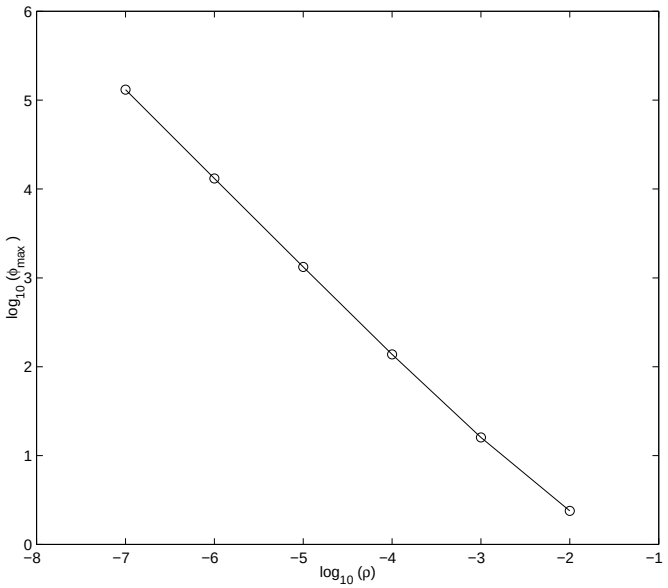

FIGURE 4.4 The reciprocal scaling of the maximum of $\phi(\tau)$ with the constant strain rate ρ, for Schnakenberg kinetics on the exponentially growing domain. The log-log plot shows that the maximum scales (approximately) as $1/\rho$.

for given initial conditions $c(x,\gamma)$ evolves such that for $\gamma \in [\gamma^*, 4\gamma^*]$ the solution is initially mode m and subsequently undergoes a transition to mode $2m$, such that the matching condition (4.28) is satisfied. Then the uniqueness of solutions of the evolution equation requires that $q_2(x,t)$ and $c(x,4\gamma)$ remain the same for $\gamma > \gamma^*$. But by construction $q_2(x,t)$ has twice the spatial frequency of $c(x,\gamma)$ and so, in the interval $\gamma \in [4\gamma^*, 16\gamma^*]$, the solution $c(x,\gamma)$ must consist of the sequence $2m$ and transition to $4m$, and so on.

In this way the pattern sequence for $\gamma > 4\gamma^*$ may be reduced to the behaviour on $\gamma \in [\gamma^*, 4\gamma^*]$. We now consider this initial interval. In particular, *if* $c(x,\gamma^*)$ consists of a pattern of mode $m = 1$ and we satisfy the matching condition to mode $m = 2$ at $\gamma = 4\gamma^*$ *then* our observations suggest that FD will naturally ensue in a self-similar cascade. Thus we need only consider the initial stages of the sequence to determine whether FD is realised—all subsequent behaviour is equivalent. Furthermore, this analysis predicts that such a sequence generated under exponential growth will undergo FD every time $\gamma \to 4\gamma$, and recalling that the scaling parameter $\gamma \propto L^2$ we see that this corresponds to doubling the length of the dimensional domain.

The stability of the solutions, for which we have shown existence, must be conjectured from the results of numerical simulations. Of course we should not need to have an exact matching (4.28) at any one instant and consequently we require some stability properties of the evolution equation. In particular we require that a solution $c(x,\gamma)$ perturbed at some point subsequent to the establishment of a large amplitude pattern remains in the vicinity of the unperturbed solution so that if $c(x,4\gamma)$ and

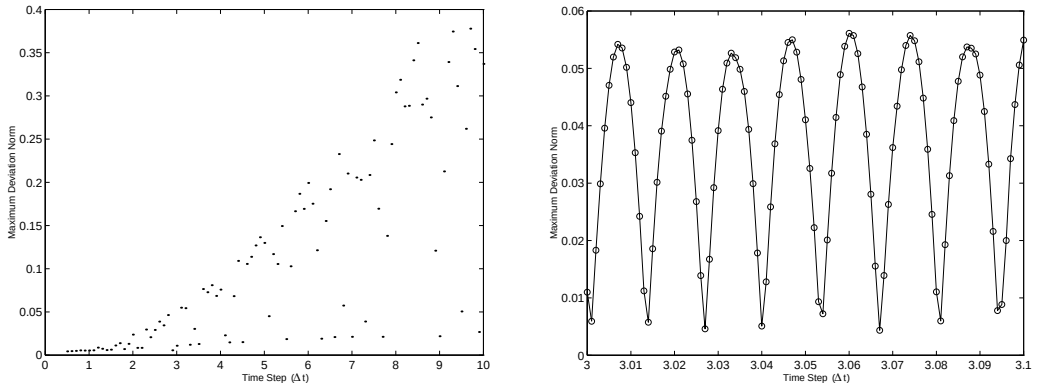

(a) (b)

FIGURE 4.5 The dependence of $\max_{x\in[0,1]} \left|c(x,\gamma) - q_2(x,\gamma/4)\right|$ during the transition between patterns as a function of the interpolation step size (see text for details). For comparison purposes the activator maximum amplitude $\eta_2 \approx 3$ during the transition. On closer inspection (b) the data are seen to oscillate. This is an artifact due to the sampling frequency and the sharpness of the transition.

$q_2(x,\gamma)$ are close at $\gamma = \gamma^*$ then they remain close during the interval $\gamma \in [\gamma^*, 4\gamma^*]$. We have performed numerical simulations of the evolution equations and have compared $c(x,4\gamma)$ and $q_2(x,\gamma)$ numerically, as described below (see also Figures 4.5(a) and 4.6), and conclude that this stability property is demonstrated by the system, at least in some range of the growth rate-determining parameter ρ. If the stability criterion is met then once some pattern is selected by the initial conditions the sequence is fully determined by the dynamics of the evolution equation and the initial conditions play no further part in determining the composition of the sequence. In this sense the patterns contained in the sequence are generated *robustly*.

We have computed $q_2(x,\gamma)$ for a solution $c(x,\gamma)$ in order to investigate the matching condition (4.28) during FD. A routine was implemented which compares the solution at time $t(\gamma)$ with the profile generated by the action of the tent map $p_2(x)$ on the solution at time $t(\gamma/4)$. To do this we use linear interpolation to approximate $c(x,\gamma/4)$, before applying the tent map to compute $q_2(x,\gamma/4) = c(p_2(x),\gamma/4)$. In Figure 4.5(a) we show how the maximum deviation over space for the activator (which is greater than the deviation for the inhibitor) depends on the time-step size. The maximum occurs during the transition between pattern modes. The time-step is simply the time interval between data records and hence the interval over which we interpolate—it does not reflect the accuracy in the time integration, which is kept constant. The figure shows that the deviation tends to zero with the step-size. This suggests that we do have $\left|c(x,\gamma) - q_2(x,\gamma/4)\right| \to 0$ during the transition, and hence the matching condition is satisfied. The transition between modes $m = 2$ and $m = 4$

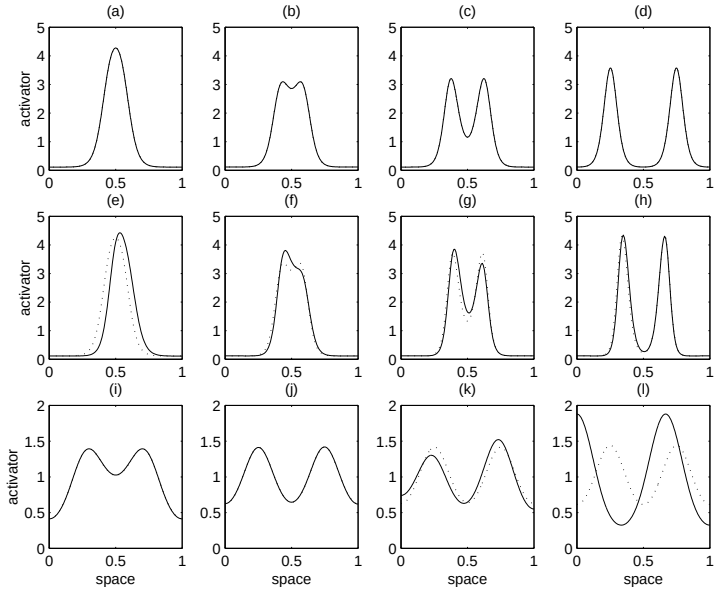

FIGURE 4.6 The peak splitting transition for three values of strain rate ρ. The transitions are from mode $m = 2$, for Schnakenberg kinetics with (a)–(d) the FD sequence for $\rho = 0.001$ and $d = 0.01$, (e)–(h) the onset of asymmetric splitting for $\rho = 0.02$ and $d = 0.01$ and (i)–(l) the breakdown in splitting behaviour for $\rho = 0.00001 < \rho_c$ with $d = 0.06$ (see text for details). The dotted trace shows the (symmetrical) tent map acting on the solution at $\gamma/4$, i.e. $q_2(x, \gamma) = c(x, \gamma/4)$ (which cannot be distinguished from the numerical solution (solid line) in (a)–(d)). At very small values of ρ correspondingly small timesteps are required numerically to investigate the solution behaviour during the transitions between patterns. Increasing d is found to raise ρ_c (see text), and in the figure we have taken $d = 0.06$ to allow a computationally reasonable timestep to be used.

is illustrated in Figure 4.6(a)–(d). Here $c(x, \gamma)$ and $q_2(x, \gamma/4)$ are plotted on the same axes and cannot be distinguished.

4.2.2 Parameter Dependence. We now look at the effect of varying parameters, and also changing various of the functional forms in the model, on the spatial frequency-doubling behaviour that we have described for exponential domain growth and Schnakenberg kinetics.

Constant Strain Rate. Numerically we find that the FD sequence is realised over several orders of magnitude of the strain rate ρ, the parameter that determines the growth rate. Here we examine the pattern sequence under exponential growth at the extremes of the range of validity of ρ. Our ability to numerically monitor FD into higher modes is severely limited by the mesh capacity that we can obtain computationally. In the current work, patterns up to mode $m = 256$ are considered in sequences of up to nine FD events. Frequency-doubling behaviour is observed under exponential growth with Schnakenberg kinetics for over four orders of magnitude in ρ for $d = 0.01$; approximately $10^{-6} < \rho < 10^{-2}$. The symmetry argument presented above would suggest that for exponential growth the sequence should persist indefinitely or fail,

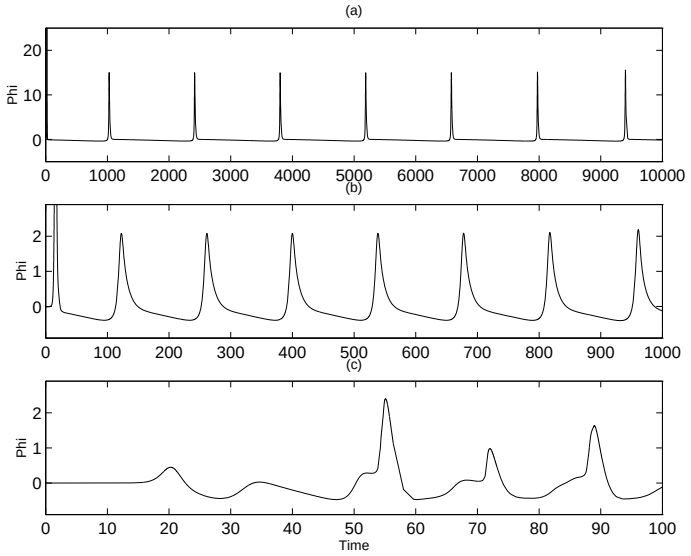

FIGURE 4.7 The departure from two characteristic dynamic regimes with increasing ρ. Timeseries for ϕ are plotted against the fast time variable t for exponential domain growth with (a) $\rho = 0.0005$, (b) $\rho = 0.005$ and (c) $\rho = 0.05$. (If plotted against the slow variable τ then all figures would have slow time (horizontal axis) on the interval $\tau \in [0, 5]$.) The early (high) peaks in (a) and (b) are initial transients.

according to whether the stability criterion is satisfied. Below we investigate this conjecture by varying the various parameters in numerical solutions of the equations.

As we let $\rho \to 1$ the timescale for domain growth converges to the timescale that was identified for pattern formation. Numerically we find that with increasing ρ an asymmetry is introduced during transition between modes of the FD sequence. For the example of Schnakenberg kinetics we find that peaks are no longer stationary before the transition to a higher mode and subsequent peak splitting is asymmetrical. The solution starts to undergo the transition before reaching a quasi-steady state. A comparison with the construction $q_2(x, \gamma/4)$, illustrated in Figure 4.6(e)–(h), shows that there is no longer matching for large ρ (as the tent map is by definition symmetrical).

The departure from the characteristic alternation between slow and fast dynamical regimes is demonstrated in the behaviour of $\phi(\tau)$, defined in section 4.1, which is shown in Figure 4.7 for three different values of ρ. The onset of the asymmetry is gradual and although the solution no longer enters a quasi-stationary state the strong tendency to peak splitting remains (for Schnakenberg kinetics), with the number of turning points on the domain continuing to double roughly periodically for some further range of ρ. When ρ becomes very large, $\rho \sim 1$, the solution is purely transient with no patterns recognisable as quasi-stationary modes. The changing form of the activator solutions with increasing ρ is shown in Figure 4.8.

Perhaps a more surprising result is that there is an also abrupt change in behaviour when ρ is decreased through a lower critical value, ρ_c. For ρ below this point the pattern sequence does not undergo FD and different sequences may be obtained for

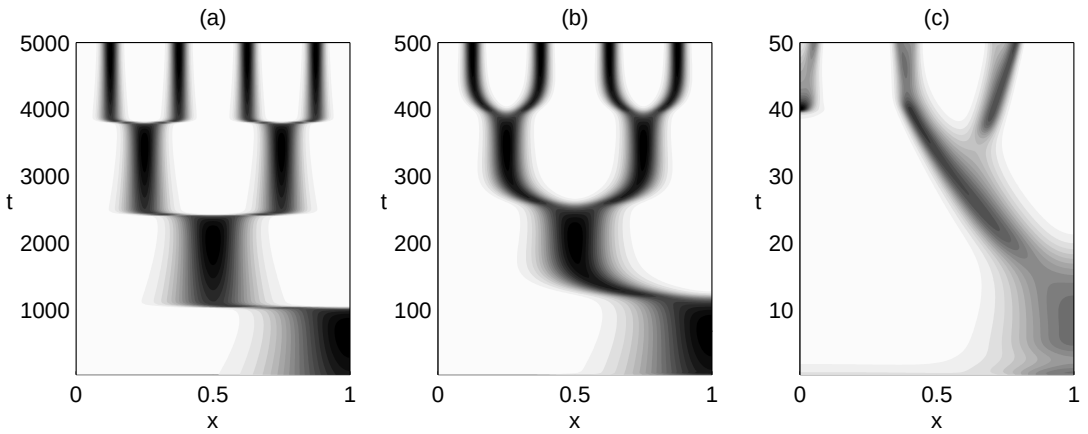

FIGURE 4.8 The loss of the FD sequence with increasing ρ. Activator solutions $v(x,t)$ are plotted for three values of the strain rate ρ for Schnakenberg kinetics and exponential domain growth. Parameters correspond to Figure 4.7 with (a) $\rho = 0.0005$, (b) $\rho = 0.005$ and (c) $\rho = 0.05$. The duration of the transitions is approximately the same in each case. In (c) the FD sequence is no longer observed. Shading is on a scale from white (0) to black (5).

different sets of initial conditions. Figure 4.6(i)–(l) illustrates the manner in which this breakdown occurs during a transition. This implies that there is a maximum timescale for domain growth beyond which the constraint imposed by the non-autonomy is not sufficient to generate the FD sequence. We note that for sequences for $\rho < \rho_c$, where the FD breaks down, $\phi(t)$ shows the same quasi-static and fast transition behaviour as for FD, however, the transitions no longer occur periodically in time.

Ratio of Diffusivities. It is of interest to see how the lower bound on ρ for FD and the onset of asymmetrical splitting as $\rho \to 1$ depend on d, the ratio of activator to inhibitor diffusivity. Numerically, we find that by increasing d (such that the diffusivities for activator and inhibitor move closer together) we also raise the lower bound, for example $\rho_c \approx 3 \times 10^{-4}$ for $d = 0.05$ compared to $\rho_c \approx 10^{-6}$ for $d = 0.01$. At the opposite end of the range of ρ for which FD is observed, as $\rho \to 1$, we find that as d is increased peaks move apart more quickly subsequent to splitting, thus delaying the onset of asymmetric transitions. This increased rate of peak separation is illustrated in Figure 4.9. We recall that d cannot be increased through the critical value d_c for the Turing bifurcation, as discussed in section 2.3. We also note that as d is increased towards d_c the peaks become wider, as can be seen in the figure.

4.2.3 Role of the Kinetics: Peak Splitting and Peak Insertion. The symmetry analysis presented above does not depend critically on the nonlinear part of the kinetic function. From this we might infer that FD is a generic property of reaction-diffusion equations provided that the linearised kinetics permit diffusion-driven instability, and that the FD pattern sequence will be realised given the initial matching of solution and construction and the stability properties as described. Numerical solution of a

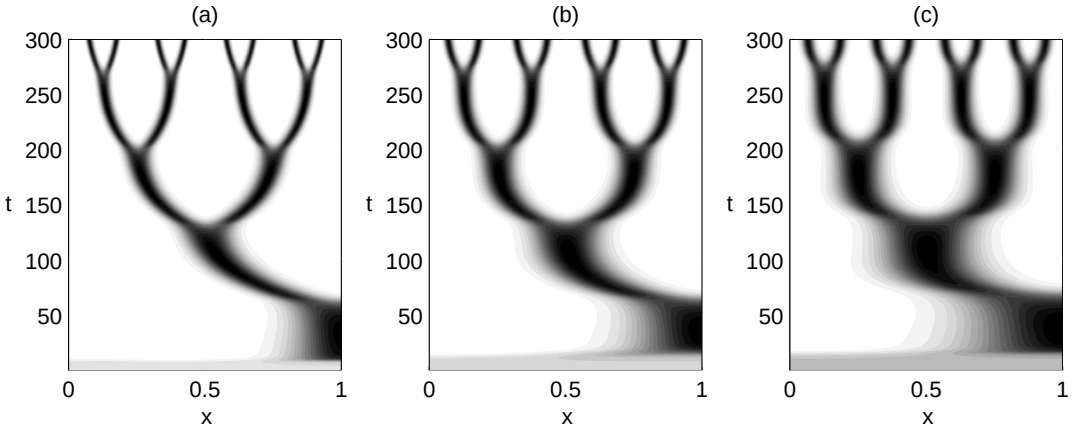

FIGURE 4.9 The dependence of the speed of peak separation on the ratio of diffusivities d, for peak separation subsequent to splitting in the FD sequence for Schnakenberg kinetics. Activator solutions $v(x,t)$ are plotted for $\rho = 0.01$ and three values of the ratio of diffusivities d on the exponentially growing domain, with (a) $d = 0.005$, (b) $d = 0.01$ and (c) $d = 0.02$. We recall that increasing d brings the diffusivities of the two species closer together. The shading scale is as for Figure 4.8.

variety of the kinetic models proposed in the literature has also produced FD sequences with either activator peak splitting, as was found for the Schnakenberg case, see Figure 4.1(a), or by activator peak *insertion*. This latter mechanism for transition between modes is demonstrated in Figure 4.10(a) for the model proposed by Gierer and Meinhardt (see Appendix A.3)

$$f(u,v) = \nu_1 v^2 - \mu_1 u \tag{4.29}$$

$$g(u,v) = \nu_2 \frac{v^2}{u} - \mu_2 v + \delta \tag{4.30}$$

and evolution equation (4.1)–(4.3). However, for this kinetic scheme we have found that when δ is identically zero the kinetics preclude FD by preventing either form of pattern reorganisation, as illustrated in Figure 4.10(b). The standard FD sequence is recovered for non-zero δ. We will investigate the mechanisms for peak splitting and peak insertion in the following chapter, and give an explanation for the singular behaviour found in the Gierer-Meinhardt model for $\delta = 0$. Also it will be shown that it is possible to generate a sequence of patterns in which activator peaks undergo splitting and insertion of new peaks *simultaneously*. This behaviour is observed for kinetic schemes which have purely cubic nonlinearity.

4.2.4 Influence of the Boundary Conditions. So far we have described pattern formation with zero-flux boundary conditions. The symmetry analysis that we have presented relies on the zero gradient at the boundary to produce solutions under the tent-mapping that are twice-continuously differentiable. However, numerical solutions show that the tendency for regular doubling of the number of peaks on the domain is not reliant on these boundary conditions. First we consider the case for periodic

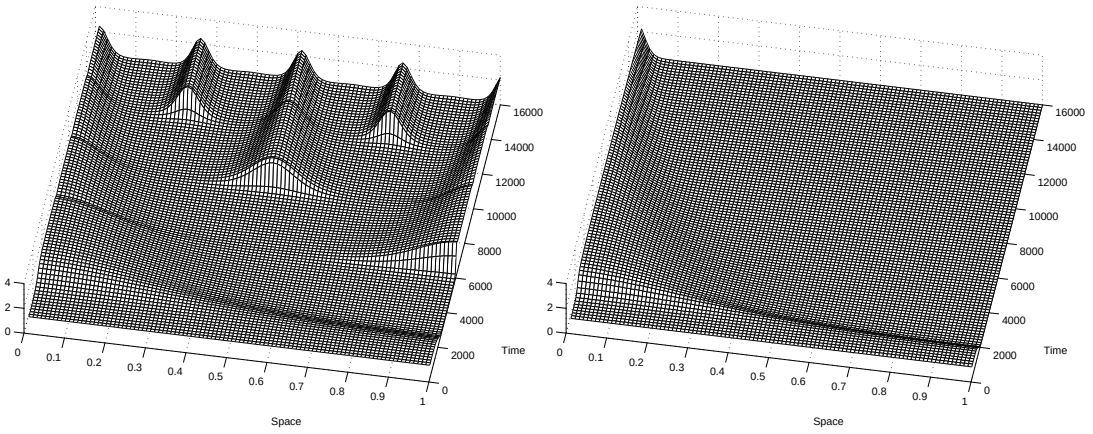

(a) (b)

FIGURE 4.10 Pattern sequence formation in the Gierer-Meinhardt model on the growing domain. Evolution of the activator species showing (a) frequency-doubling with peak insertion for with $\delta = 0.001$ and (b) the solution for $\delta = 0$ for which pattern reorganisation is precluded. Kinetic parameters $\nu_1 = \mu_1 = 0.02$ and $\nu_2 = \mu_2 = 0.01$,

boundaries, such that in one spatial dimension pattern formation is on the ring. In this case we remove boundary effects from the problem. It is clear that the half-peak pattern mode is not a solution on the periodic domain. Figure 4.11 shows the solution to equations (4.1)–(4.3) for the activator species on a periodic domain with exponential domain growth and Schnakenberg kinetics, from which we recover FD as usual. We have computed numerical solutions with periodic boundaries using an implicit differences scheme, which employs the Sherman-Morrison formula [113, p.68] to solve the sparse cyclic tridiagonal system (an augmented-tridiagonal matrix) generated by the discretisation.

Scalar boundary conditions (see section 2.1) may be written in the form

$$(\mathbf{n} \cdot \nabla)\, \mathbf{c} = P\,(\mathbf{c}^* - \mathbf{c}) \tag{4.31}$$

where $\mathbf{n}$ is the unit outward normal on the boundary. For different choices of the parameter $0 \leq P_i \leq 1$ and the external reference concentrations $\mathbf{c}^* \geq \mathbf{0}$ we move from zero flux ($P = 0$) to Dirichlet ($P = \infty$) conditions, which are homogeneous when $\mathbf{c}^* = \mathbf{c}_s$. For intermediate values of P we have inward or outward flux depending on whether the concentration at the boundary is lower or higher than the external concentration $\mathbf{c}^*$. This can be thought of as a leakage of chemical into or out of the domain.

Patterns generated on a domain of fixed size under flux-leakage boundary conditions are found by numerical simulation to be weakly perturbed from the zero flux

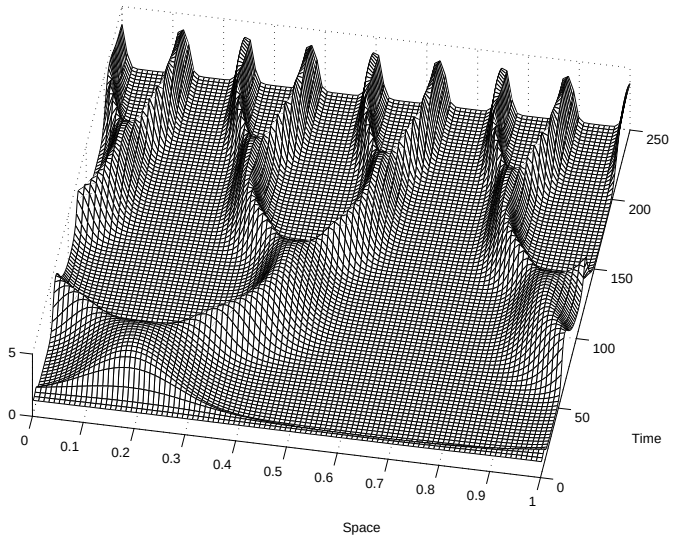

FIGURE 4.11 The FD sequence for periodic boundaries (solution on the ring). Evolution of the activator concentration profile $v(x,t)$ with exponential growth for $\rho = 0.01$ with Schnakenberg kinetics and $d = 0.01$. The initial domain size is such that $\gamma_0 = 5$.

patterns, with small lateral displacement of peaks and modification in the peak profile. Inward flux at the boundaries is found to displace peaks towards the centre of the domain, while outward flux pushes peaks towards the boundaries. This result for outward flux is observed for $\mathbf{c}^* = \mathbf{0}$ for which

$$(\mathbf{n} \cdot \nabla)\, \mathbf{c} = -P\mathbf{c} \tag{4.32}$$

where, for example, we might take $P = 1/2$ (and the concentrations $c_i > 0$ always). For inward flux conditions we choose $\mathbf{c}^* > \mathbf{0}$ and sufficiently large that $c_i^* - c_i > 0$ always. On the growing domain these boundary conditions give rise to regular doubling in the number of peaks on the domain, and cause only small quantitative perturbations to the FD sequence for zero flux conditions. Furthermore, for these boundary conditions the initial pattern to develop is found to be the centralised peak, rather than the boundary peak. For Dirichlet conditions, $P = \infty$, with values of $\mathbf{c}^*$ such that pattern modes are admitted as solutions of the evolution equation, the same strong tendency to frequency-doubling behaviour is observed.

4.3 Three-Species Models

In Turing's original paper, and in most of the subsequent discussion and application of the theory in biological and non-biological contexts alike, only two interacting species are considered.[2] In two-species models it is straightforward to show that temporal oscillations cannot occur with diffusion-driven instability. (The homogeneous steady

[2]For a single diffusing substance with nonlinear kinetics there can be no homogeneous state, stable to homogeneous disturbance, which is unstable to spatially heterogeneous perturbations. Heterogeneous

state may of course lose stability to spatially homogeneous oscillations through Hopf bifurcation in the kinetic term.) However, for three or more interacting species it is possible to induce spatio-temporal oscillations driven by diffusion.

Various authors have studied model systems with more than two components. Othmer and Scriven [101] consider the stability of the homogeneous state in n-component systems, allowing cross-diffusion (such that the off-diagonal elements in the matrix of diffusivities are non-zero). The authors find that for two-species systems with cross-diffusion then it is possible to excite oscillatory instabilities, however, there is no fastest growing wavenumber in this case (i.e. the complex solutions to the dispersion relation, $\lambda(k^2)$, have positive real part which is monotonically increasing with wavenumber). In general standard linear analysis becomes intractable for n-component systems where $n > 3$ due to the fact that stability is determined by eigenvalues which are the roots of an n^{th}-degree polynomial. It is interesting to consider what generalisations to the concepts of short-range activation and long range inhibition arise in these systems. Where three or more components interact it may be possible to divide the system into weakly-interacting subsystems of two or three components [101]. Furthermore it may be sufficient to consider the interaction of subsystems that behave collectively in an inhibitory or activatory manner to derive necessary and sufficient conditions for instability (R. Satnoianu, *pers. comm.*).

There is no *a priori* reasoning to suggest that models of putative biological interest should be restricted to two-species systems. Below we take from the literature a model describing the interaction of a three component system which gives rise to patterns through the Turing instability and which can give stationary spatial patterns and time-oscillating patterns as model parameters are varied. White and Gilligan [131] propose the model for the interaction of a host-parasite-hyperparasite system, such as a cereal root complex infested with a parasite into which a biological control agent (hyperparasite: fungi, bacteria or other microorganism) has been introduced, to account for spatial patchiness in population density. A brief derivation of the model is presented in Appendix A.4, however, here we are primarily interested in the solution behaviour, rather than in the biological details.

The population dynamics is described by local interaction terms and diffusion is assumed to model the spatial spread and dispersion of each species. The nondimensional equations for host (v), parasite (w) and hyperparasite (u) on the growing domain are

$$u_t = \frac{1}{\gamma(t)} u_{xx} - \delta\,(u - w) - \rho\sigma(t)u \tag{4.33}$$

$$v_t = \frac{d_v}{\gamma(t)} v_{xx} + v\left(1 - \frac{v}{\kappa}\right) - vw - \rho\sigma(t)v \tag{4.34}$$

solutions may, however, be admitted in scalar reaction-diffusion equations, but not through the Turing instability (see Grindrod [46]).

$$w_t = \frac{d_w}{\gamma(t)} w_{xx} + \mu \left(v \frac{w}{1+\beta} - u \frac{w}{1+\beta w} \right) - \rho\sigma(t) w \tag{4.35}$$

where δ, κ, μ and β are nondimensional kinetic parameters and for slow uniform growth γ changes, as before, according to equation (4.3). The boundary conditions are zero flux at $x = 0, 1$, and we impose random initial conditions. First we consider parameters such that on the static domain (where $\rho = 0$ so that $\gamma = \gamma_0$) a stationary pattern develops through the diffusion-driven instability. Considering the Jacobian (around the stable fixed point of the kinetic system) we find

$$\mathcal{A} = \begin{pmatrix} -\delta & 0 & \delta \\ 0 & -\dfrac{v_s}{\kappa} & -v_s \\ \dfrac{\mu v_s}{1+\beta} & \dfrac{\mu u_s}{1+\beta} & \dfrac{\mu\beta v_s^2}{(1+\beta)^2} \end{pmatrix} \tag{4.36}$$

where the kinetic steady state values u_s and v_s are positive. Thus the Jacobian has the sign structure

$$\operatorname{sgn}(\mathcal{A}) = \begin{pmatrix} - & 0 & + \\ 0 & \begin{bmatrix} - & - \\ + & + \end{bmatrix} & \end{pmatrix} \tag{4.37}$$

so that w is self-activating, and in particular the interactions between v and w are those required for DDI with cross-kinetics in the two species problem (highlighted in the square brackets). Hence we may expect that if the diffusivities of v and w are sufficiently different then this subsystem alone may be sufficient to give rise to stationary heterogeneous pattern, without any further destabilising influence of u. Indeed, if we take $d_w \ll d_v \approx 1$ then we can recover stationary patterns in the three species, as shown in Figure 4.12(a). Here w takes role of activator (and has the largest amplitude pattern) and v is the inhibitor (which is out of phase with w for the cross-kinetic system). We do not present any further analysis of DDI in this system here but refer the reader to White and Gilligan [131].

Considering the model on the growing domain, we find that in this regime the patterns evolve by peak splitting of species w (the activator) in an analogous manner to the two species examples studied in the previous section. A numerical solution for the activator species w is shown in Figure 4.12(b).

If the ratios of diffusivities are changed so that d_v and d_w are not significantly different in magnitude but are both small (in comparison to $d_u \equiv 1$), then we cannot make the above inferences. In fact it is possible to excite spatially heterogeneous instabilities which oscillate in time under such conditions. In this case, on the static domain the long-time behaviour of the system is oscillatory, with a timescale that is intrinsic to the equation parameters. The time-varying solution $w(x,t)$ for the model under these conditions is plotted in Figure 4.13(a). The oscillations for u and w are

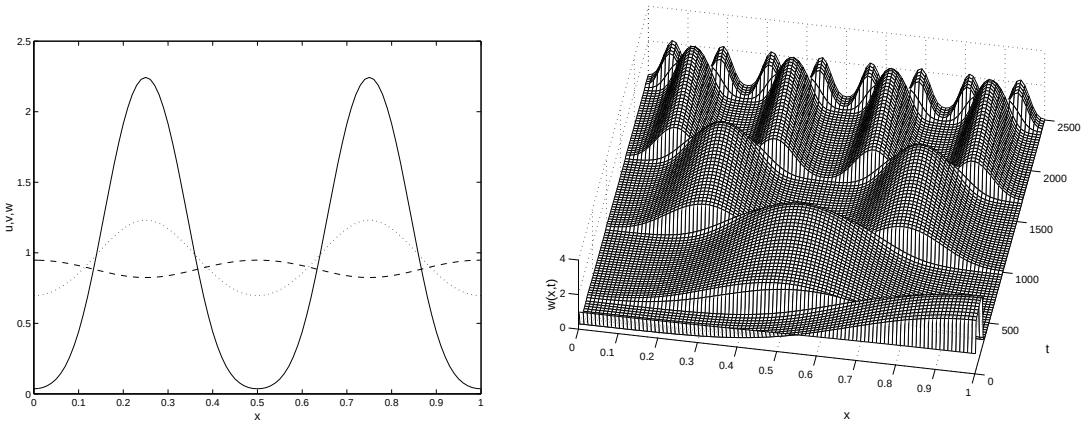

(a) (b)

FIGURE 4.12 Pattern formation for non-oscillatory solutions in the three-species model of White and Gilligan. In (a) we plot $u(x)$ (dotted), $v(x)$ (dashed) and $w(x)$ (solid) steady state patterns for the stationary domain with $\gamma_0 = 10$ and in (b) we plot the evolving profile $w(x,t)$ on the growing domain with $\rho = 0.001$ and $\gamma_0 = 1$. Kinetic parameters are $\kappa = 10$, $\mu = 15$, $\delta = 5$ and $\beta = 4$ with ratios of diffusivities $d_v = 1.0$ and $d_w = 0.05$.

out of phase with those of v. The frequency of oscillation is approximately 0.1 nondimensional units.[3] It is interesting to ask what effects the interaction of the timescale for domain growth has with the timescales for pattern oscillation and pattern formation linear growth. The timescale for slow domain growth is much longer than that for oscillation so that the patterns will not be quasi-stationary when transitions are initiated. Solutions for $\rho = 0.01$ are shown in Figure 4.13(b)–(d). We choose a value for ρ at the high end of 'slow' domain growth because the timestep required to compute the oscillation is correspondingly small. Similar behaviour is observed for lower values of ρ. The simulations show that the solution no longer undergoes the simple FD behaviour shown in the previous case. The solution becomes increasingly complicated, and pattern appears to move in an increasingly (oscillatory) wave-like manner from the centre outwards. At later times the behaviour becomes quite irregular and asymmetric. This increased complexity might be expected as the effect of introducing a third timescale into the problem.

There are no qualitatively new phenomena which can arise from the diffusion-driven instability when systems of more interacting components are considered. The three-species problem illustrates both stationary and oscillatory spatial patterns, which introduce a new timescale through the oscillation. On the growing domain, this third

[3]The ratios of diffusivities in Figure 4.13(a) are $d_v = 0.04$ and $d_w = 0.005$, however, similar results are recovered for $d_w = 0.02$, as used by White and Gilligan. The period of the oscillations is $T \approx 11$ nondimensional time units. This is contrary to the period of oscillation reported by White and Gilligan, which is on the order of 10^2 too large, probably due to under sampling arising from too large a timestep in their simulation.

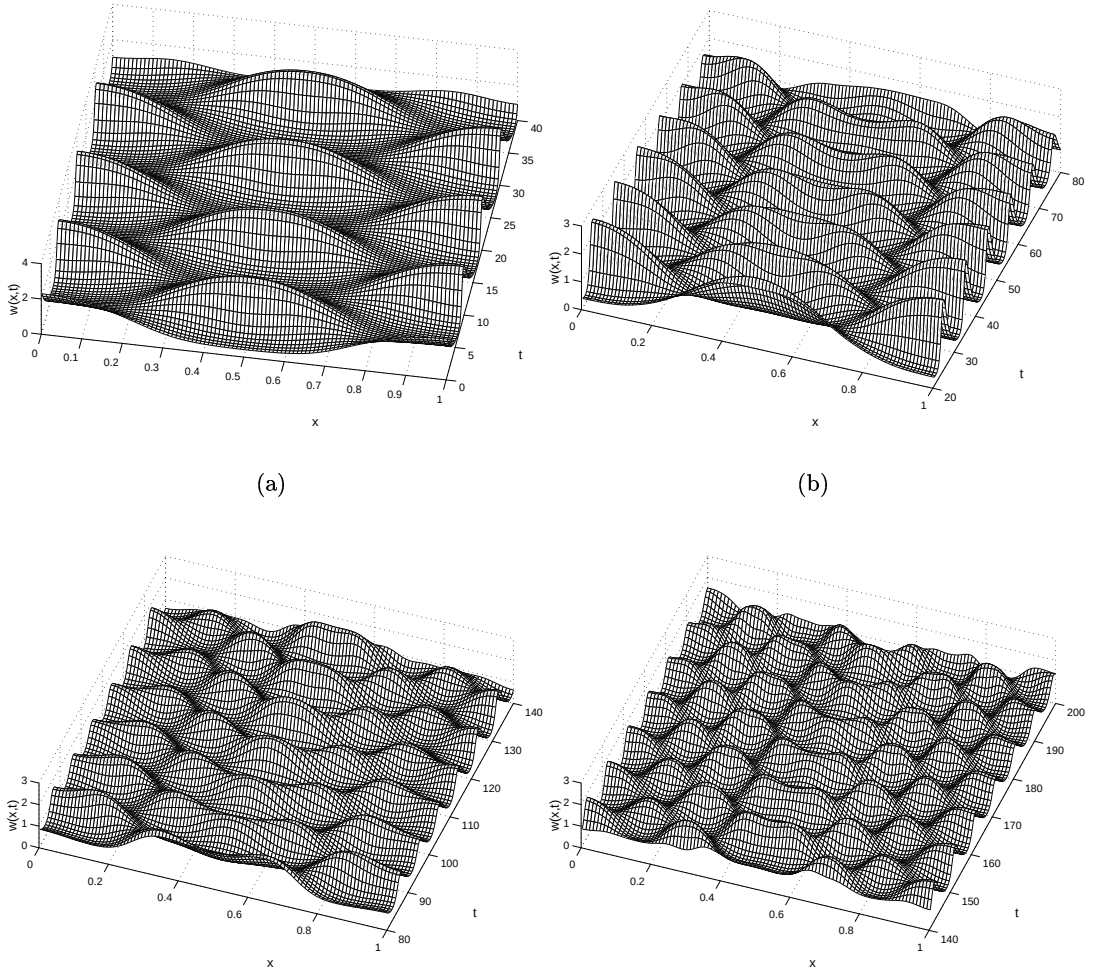

FIGURE 4.13 Oscillating patterns in the three-species model of White and Gilligan (a) on the static domain and (b)–(d) evolution of oscillating pattern on the growing domain, with (b) $t \in [20, 80]$, (c) $t \in [80, 140]$ and (c) $t \in [140, 200]$. Kinetic parameters are $\kappa = 500$, $\mu = 2$, $\delta = 2$ and $\beta = 4$ with ratios of diffusivities $d_v = 0.04$ and $d_w = 0.005$. In both cases $\gamma_0 = 25$ and for the growing domain $\rho = 0.01$.

timescale interacts with those already in the problem, the timescales for pattern growth and domain growth, and underlies the difference in behaviour between these two cases.

4.4 Other Domain Growth Functions

For a tissue expanding locally under constant strain rate the growth is exponential. This may be considered to model a population of cells dividing at a fixed rate which is independent of spatial or temporal coordinate. While this may be a reasonable model of the initial stages of an unconfined growth it is not realistic for many biological applications. We wish to know if the functional form of the domain growth has any bearing on the pattern sequence generated. We can use the symmetry analysis to investigate pattern formation under other functional forms for the domain growth. In previous studies various authors have considered linear growth. Although this may not have a strong biological motivation, studying this growth function gives further insight into the mechanism of pattern sequence formation. We also consider the biologically plausible scenario of logistic time dependence, where the final domain attained is limited to some finite size.

4.4.1 Linear Growth. Uniform linear domain growth, which we define by $r(t) = 1 + \rho t$, may be generated by the time-varying strain rate

$$S(t) = \rho\sigma(t) = \frac{\rho}{1+\rho t}. \tag{4.38}$$

We apply the previous analysis to the problem with explicit linear growth. Again t is eliminated, writing

$$\gamma(t) = \gamma_0(1+\rho t)^2, \quad h(\gamma) = \frac{d\gamma}{dt} = 2\rho\sqrt{\gamma_0\,\gamma} \tag{4.39}$$

so that $h(4\gamma) = 4\rho\sqrt{\gamma_0\gamma} = 2h(\gamma)$, which does not satisfy the condition (4.26). For convenience we will take $\gamma_0 = 1$. As before we examine the evolution of a pattern over some interval $[\gamma, 4\gamma]$. On eliminating t the governing equation for $c(x, 4\gamma'; \rho)$ is

$$\rho\sqrt{\gamma'}\frac{\partial c}{\partial \gamma'} = \frac{d}{4\gamma'}\frac{\partial^2 c}{\partial x^2} + R(c) - \frac{\rho c}{2\sqrt{\gamma'}}. \tag{4.40}$$

Again we consider the frequency-doubling construction, while this time allowing for a change in ρ to find the equivalent equation. Now $q_2(x, \gamma'; \rho') \equiv c(p_2(x), \gamma'; \rho')$ satisfies

$$2\rho'\sqrt{\gamma'}\frac{\partial q_2}{\partial \gamma'} = \frac{d}{4\gamma'}\frac{\partial^2 q_2}{\partial x^2} + R(q_2) - \frac{\rho' q_2}{\sqrt{\gamma'}} \tag{4.41}$$

so that $q_2(x, \gamma; \rho/2)$ and $c(x, 4\gamma; \rho)$ are shown to satisfy the same equation.

The implication of this result is that prolonged FD behaviour is not a natural consequence of this growth function. However, as before, if there exists a point $\gamma = \gamma^*$ such that

$$q_2(x, \gamma^*; \rho/2) = c(x, 4\gamma^*; \rho) \tag{4.42}$$

then $q_2(x, \gamma; \rho/2)$ and $c(x, 4\gamma; \rho)$ coincide for all $\gamma > \gamma^*$. This implies that if a sequence generated with linear growth rate ρ undergoes N frequency-doubling events before this sequence breaks up, then a sequence generated at growth rate 2ρ must complete $N + 1$ such events. Again we conjecture that stability properties are inherited from the results of numerical simulations. Numerical evidence confirming this prediction for one such regime is presented in Figure 4.14. Although the analysis does not give any information about the sequence after the breakdown of FD, numerical solutions suggest that the subsequent behaviour is not robust, and the sequence may be different for each set of initial conditions.

4.4.2 Comparisons with Exponential Domain Growth. For slow pattern evolution in the quasi-steady regime the timescale for pattern formation must be sufficiently faster than that for domain growth. We can predict the point of breakdown of the frequency-doubling sequence under linear growth conditions from knowledge of the lower limit in the rate-determining parameter, ρ_c, for the sequence under exponential growth. Comparison of growth rates then suggests that FD will occur for linear growth while

$$h_{lin}(\rho) \geq h_{exp}(\rho_c) \tag{4.43}$$

where $h_{exp} = 2\rho\gamma$ and $h_{lin} = 2\rho\sqrt{\gamma\gamma_0}$, which gives frequency-doubling for

$$\gamma \leq \gamma^* \equiv \gamma_0 \left(\frac{\rho}{\rho_c}\right)^2 \tag{4.44}$$

and the FD behaviour is expected to break down for γ above γ^*. This value is indicated by the vertical dashed line in Figure 4.15. Numerical simulations have confirmed that for linear domain growth the value of γ for breakdown varies approximately with the square of ρ. From equation (4.44) we see that higher pattern modes (for which we require large γ^*) may be admitted prior to the breakdown of the sequence only if ρ is sufficiently larger than ρ_c. Then from the first of (4.39) the sequence is expected to break down for times t where

$$t > t^* \equiv \frac{1}{\rho_c} - \frac{1}{\rho} \approx \frac{1}{\rho_c} \tag{4.45}$$

which, for $\rho_c \approx 10^{-6}$, gives the correct order of magnitude for the results of numerical simulations shown in Figure 4.14.

For large ρ, analogously to the exponential case, breakdown of FD occurs as $\rho \to 1$ through the introduction of an asymmetry during transitions between low modes. This happens as the timescales for pattern formation and domain growth coincide and the distinction between slow and fast dynamics regimes for the evolution is eroded.

4.4.3 Logistic Growth. If the sensitivity of the tissue to the patterning mechanism is confined to a phase of exponential growth, then the previous results are sufficient to predict the patterning behaviour. However, if pattern is organised during the period

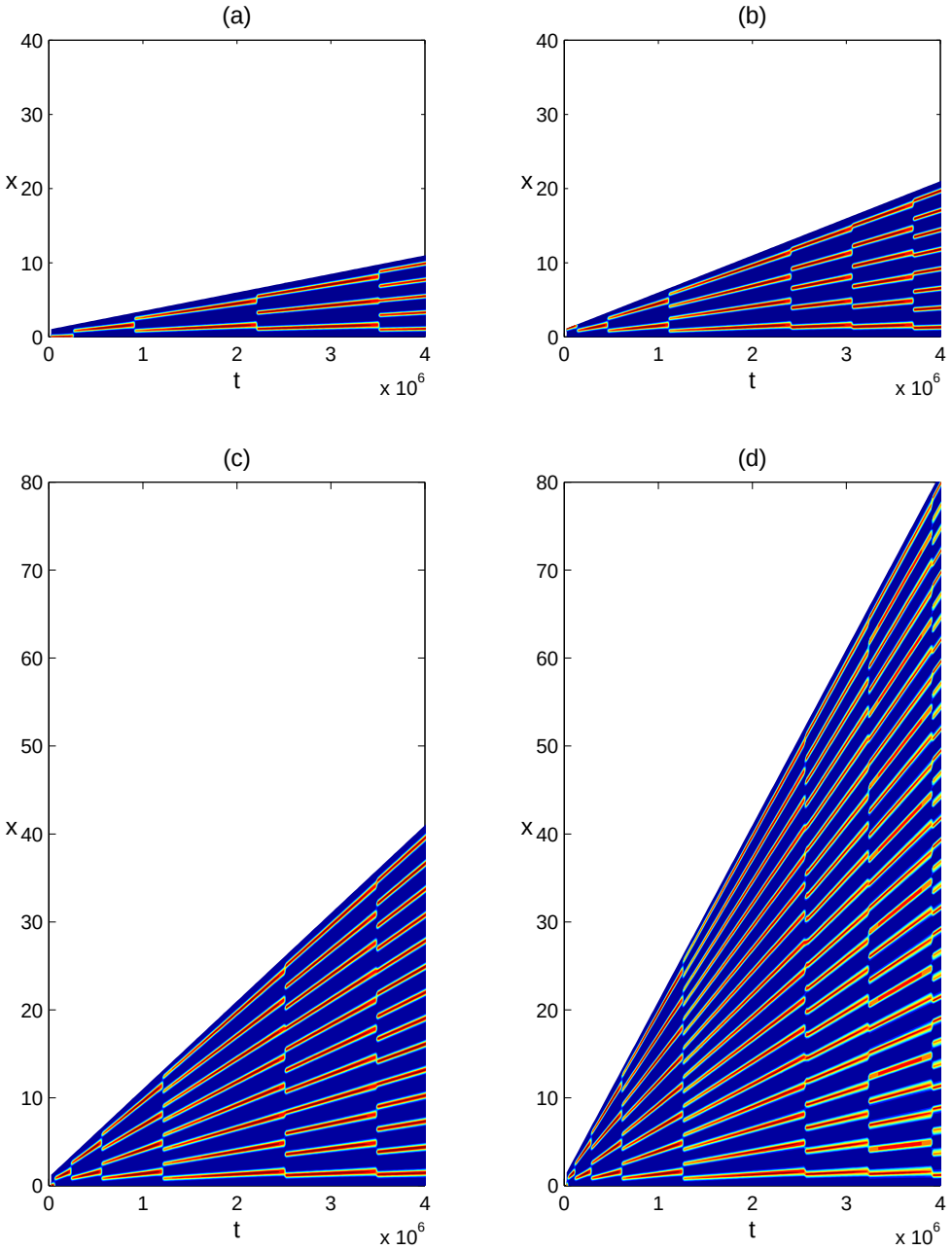

FIGURE 4.14 Pattern sequences under linear domain growth. The evolution of the activator concentration profile $v(x,t)$ with Schnakenberg kinetics for (a) $\rho = 2.5 \times 10^{-6}$, (b) $\rho = 5.0 \times 10^{-6}$, (c) $\rho = 1.0 \times 10^{-5}$ and (d) $\rho = 2.0 \times 10^{-5}$, with $\gamma_0 = 1.0$, showing 2, 3, 4 and 5 frequency-doubling transitions respectively before the sequence breaks down. Transitions appear discontinuous because they occur over a time interval much smaller than the total interval shown in the figures. Other simulations have shown that subsequent to breakdown of FD the pattern sequence is non-robust both as to the component modes in the sequence and as to when the transitions occur.

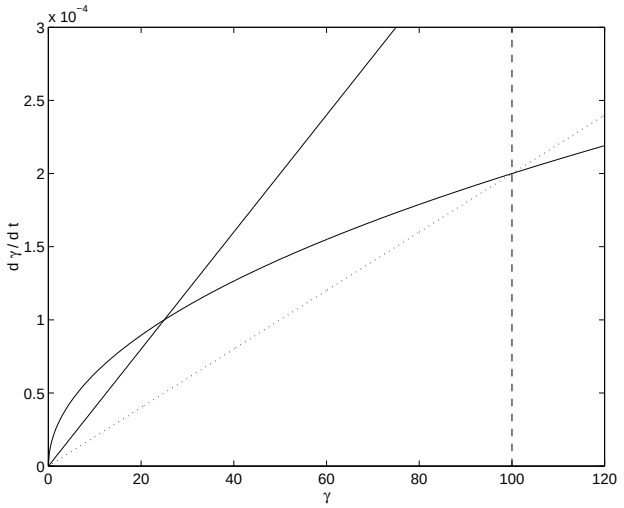

FIGURE 4.15 Illustration of the condition (4.44). The rate of change of γ is plotted against γ for exponential (straight line) and linear (curved line) growth functions. The intersection (marked with vertical dashes) between the linear growth curve and the line for exponential growth at the (lower) critical rate parameter ρ_c (dotted line) gives the approximate value of γ after which the FD sequence is expected to break down for linear growth. The straight solid line represents exponential growth for $\rho > \rho_c$ for which frequency-doubling is observed.

over which the domain growth slows and saturates to achieve some final domain size then we wish to see how this affects pattern formation, and in particular the robustness of the sequence and final pattern that is obtained. Therefore we consider pattern formation under a (spatially uniform) logistic growth function

$$r(t) = \frac{\zeta \exp(\rho t)}{\zeta + \exp(\rho t) - 1} \tag{4.46}$$

such that $\mathrm{d}r/\mathrm{d}t = \rho r(1 - r/\zeta)$, where ζ is the ratio of final to initial length. This may be generated from a local time varying strain rate with time dependence

$$S(t) = \rho\sigma(t) = \frac{\rho\,(\zeta - 1)}{\zeta + \exp\,(\rho t) - 1}. \tag{4.47}$$

In Figure 4.16(a) we show the results of a numerical simulation for logistic domain growth in which mode $m = 16$ persists at the final domain size. We have chosen the rate parameter ρ to be relatively large such that the transitions between patterns are shown to be smooth. The logistic growth is initially exponential in form, but slows to asymptotically approach the final domain length. If we are in the range for which exponential and linear growth functions give FD then we might expect, for a given ρ and for most ζ, that one constituent mode of the FD sequence will persist as the domain tends asymptotically to its final length. However, if ζ is such that the sequence begins to undergo reorganisation during the asymptotic approach to the final domain size, then some other mode may be admitted and non-robust pattern selection may occur. We will seek to ascertain the relative size of the interval in ζ in which another

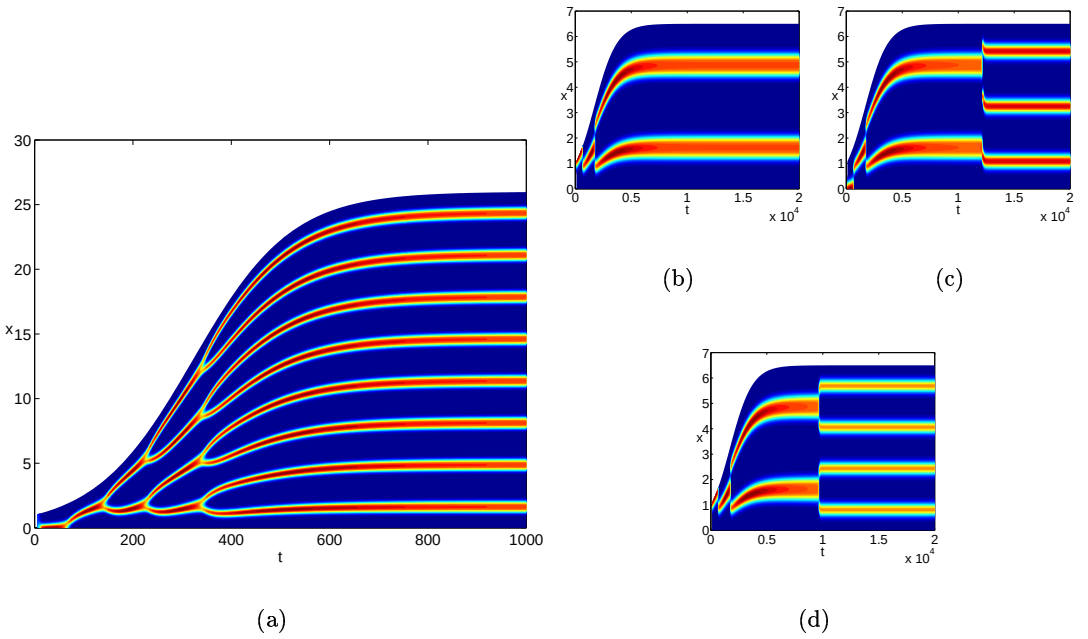

FIGURE 4.16 Pattern sequences under logistic growth. Evolution of activator concentration profile $v(x,t)$ with Schnakenberg kinetics for logistic growth with (a) $\rho = 0.01$ and $\zeta = 26.0$ showing selection of mode $m = 16$ from the FD sequence. The short interval in ζ for which other patterns are admitted is illustrated for $\rho = 0.001$ with (b) $\zeta = 6.50 \approx \zeta_4^{max}$ selecting $m = 4$, (c) $\zeta = 6.51$ for which the final pattern is $m = 6$, not in the FD sequence, and (d) selection of $m = 8$ for $\zeta = 6.52 \approx \zeta_8^{min}$. Solutions are for Schnakenberg kinetics.

mode, not an element of the foregoing FD sequence, is the final pattern mode selected as the domain tends to its final size.

If, for given ρ, a particular mode m of the FD sequence persists to the final domain length for the interval $\zeta \in [\zeta_m^{min}(\rho), \zeta_m^{max}(\rho)]$, then the existence of a window of non-robust behaviour implies that $\zeta_{2m}^{min} > \zeta_m^{max}$. The probability of observing a final pattern which is not of the FD sequence will depend on the relative sizes of $\mathcal{R}_m = \zeta_m^{max} - \zeta_m^{min}$ and $\mathcal{N}_{m,2m} = \zeta_{2m}^{min} - \zeta_m^{max}$, intervals of robust and non-robust pattern selection respectively, which will depend on m and ρ. Numerically we can estimate ζ^{max} and ζ^{min} for different modes through repeated simulations for different values of ζ and hence calculate estimates for $\mathcal{N}_{m,2m}$ and $\mathcal{R}_m$. Such estimates for $\rho = 0.001$ and $d = 0.01$, taken from a series of numerical simulations, are presented in Table 4.1. These data show that intervals of non-robust pattern selection $\mathcal{N}$ are over two orders of magnitude smaller than the intervals, $\mathcal{R}$, for which the final pattern is from the FD sequence. Figure 4.16(b)–(d) illustrates the final pattern selection over a small interval in ζ, with the final pattern moving from mode 4 to 8. The window of non-robust behaviour exists but is relatively very small. We find in the window $\mathcal{N}_{m,2m}$ that we get modes between m and $2m$, usually we see even modes (internalised peaks)

mode m	1	2	4	8	16	32	64
ζ_m^{min}	–	1.63	3.26	6.52	13.03	26.09	52.43
ζ_m^{max}	1.62	3.25	6.50	13.00	26.04	52.33	106.60
$\mathcal{R}_m = \zeta_m^{max} - \zeta_m^{min}$	–	1.62	3.24	6.48	13.01	26.24	54.17
$\mathcal{N}_{m,2m} = \zeta_{2m}^{min} - \zeta_m^{max}$	0.01	0.01	0.02	0.03	0.05	0.10	–

TABLE 4.1 Windows of non-robust pattern selection for logistic domain growth. The table contains numerical estimates (± 0.01) for the critical values of ζ (defined in the text) for various modes, under logistic growth with $\rho = 0.001$, $d = 0.01$ and Schnakenberg kinetics. Numerical solutions were computed to large time to reliably estimate ζ_{min}.

for Schnakenberg, although much less frequently we do observe odd mode patterns. Within the window it seems that for a given $\zeta \in [\zeta_m^{max}, \zeta_{2m}^{min}]$ one can get different final modes between m and $2m$ for different sets of initial conditions.

Numerical simulations also allow us to investigate how the windows of non-robustness depend on the parameters d and ρ. The numerical estimates of ζ_m^{max} and ζ_m^{min} for different combinations of these two parameters for the transition between modes 4 and 8 are shown in Table 4.2. These data suggest that the window $\mathcal{N}_{4,8}$ shrinks with increasing ρ (as the domain growth rate is increased) while the beginning of the window in ζ does not move as ρ is varied. However, when the ratio of diffusivities is increased towards d_c the window grows, while the onset is delayed by increasing d. Over the range of d and ρ tested, the window still remains much smaller than the range of ζ for which the pattern from the FD sequence is selected.

4.4.4 Hysteresis. The model (4.1)–(4.3) exhibits hysteretic behaviour, which appears to be generic and not dependent on the particular kinetic scheme, and which is manifest in two ways. Firstly the equations show the simple hysteretic effect of an S-shaped bifurcation curve, giving bistability over some range of the parameter (here γ). Secondly, the actual sequence of patterns generated changes for a shrinking as opposed to a growing domain, over some wider range of γ. We investigate these phenomena with a concrete example, by considering an explicit time dependence. An exponentially increasing and decreasing domain size is given by

$$\gamma(t) = \begin{cases} \gamma_0 \exp(2\rho t), & t < t' \\ \gamma_0 \exp\left(2\rho\,(2t' - t)\right), & t \geq t' \end{cases} \tag{4.48}$$

so that $\gamma(0) = \gamma(2t') = \gamma_0$. Firstly we show hysteresis in the transition between two modes. For this purpose we consider the transition between modes $m = 1$ and $m = 2$, which avoids the complication of intervening modes. The amplitude of the activator profile $v(x,t)$, $\eta_2(\gamma)$, while increasing and decreasing γ according to (4.48) through the transition between modes, is plotted in Figure 4.17. The beginning and end points are the same, but the onset of the down-mode transition is delayed on decreasing γ, showing the hysteretic effect.

ρ	d	ζ_4^{max}	ζ_8^{min}	$\mathcal{N}_{4,8}$
0.001	0.01	6.500	6.512	0.012
0.0001	0.01	6.499	6.559	0.060
0.01	0.01	6.500	6.507	0.007
0.001	0.005	6.335	6.338	0.003
0.001	0.02	6.789	6.852	0.063

TABLE 4.2 The dependence of the onset and interval length of windows of non-robust pattern selection on model parameters. The table shows numerical estimates for ζ_4^{max} and ζ_8^{min} under logistic domain growth with various ρ and d. The approximate error in the ζ values is ± 0.001, and in the calculated $\mathcal{N}$ is ± 0.002.

For transitions at higher mode, where intervening modes are skipped, there is no guarantee that on decreasing γ the same sequence will be followed. In fact we find that in general a different set of patterns is observed, with a tendency to include a greater number of modes sequentially. An example is presented in Figure 4.18. The reasons underlying these hysteretic effects will be discussed in the next chapter.

4.5 Domain Growth is a Mechanism for Reliable Pattern Selection

The FD sequence that we have studied for slow uniform domain growth in one spatial dimension provides a mechanism by which pattern modes may be selected robustly. Our numerical results suggest that the frequency-doubling behaviour (whether by splitting or insertion) is generic to reaction-diffusion systems which generate spatial pattern through the Turing instability, and that the sequence is not destroyed by varying the boundary conditions from zero-flux. The sense in which patterns in the sequence are robustly generated is that once initiated, the sequence of patterns unfolds with no dependence on the initial conditions. Once a large amplitude pattern is established the dynamics are governed by the change in γ. We have shown that logistic domain growth can reliably (although not perfectly) select one pattern from a sequence which persists as the domain tends asymptotically to its final size.

Semi-scale Invariance. On a domain of fixed size, pattern selection depends strongly on the domain length and multiple patterns may be admissible for a particular length for different sets of initial data. For the FD sequence the situation is quite different. The pattern sequences capture a degree of insensitivity to domain length, with each pattern element in the sequence persisting while the domain *doubles* in length. This *semi*-scale invariance is particularly significant in that it allows regulation, whereby a specific number of pattern elements is laid down despite significant variation in the domain size and without need to finely tune parameter values. Previous attempts to achieve scale invariance in reaction-diffusion systems have all required feedback from the domain size to the kinetic parameters in the model [100, 52]. The semi-scale invariance demonstrated on the growing domain arises as a natural consequence of the mechanism by which pattern sequences are formed.

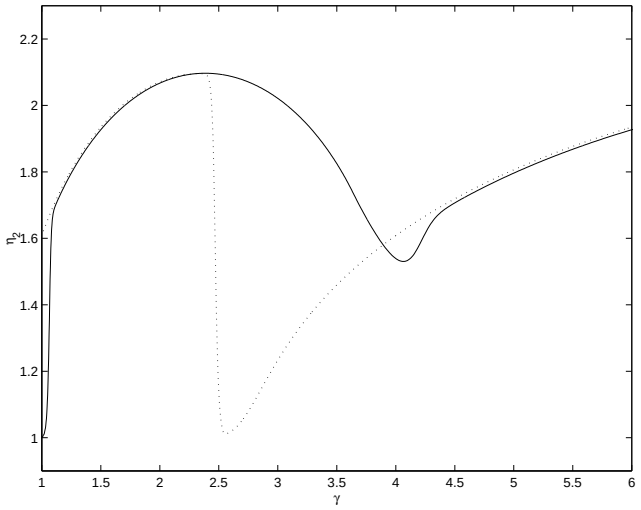

FIGURE 4.17 Hysteresis in a single transition for exponential domain growth and contraction. The maximum amplitude, $\eta_2(t)$, for the activator is plotted for increasing (solid) and decreasing (dotted) γ, both parameterised by time t. The domain growth and contraction has $\rho = 0.001$ for $\gamma(t)$ given by equation (4.48) with $\gamma_0 = 1$ and $t' = 1000$. We use Schnakenberg kinetics and $d = 0.01$.

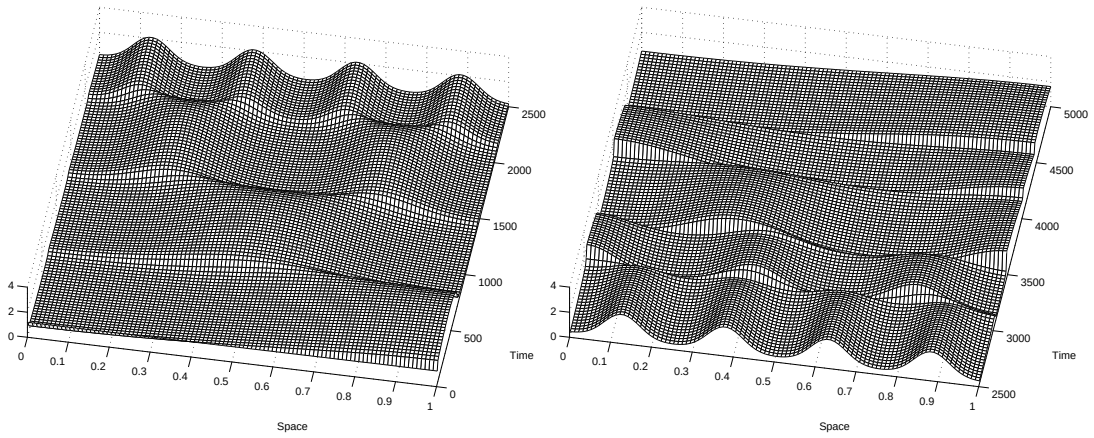

(a) (b)

FIGURE 4.18 Hysteresis in the pattern modes comprising the sequence for exponential domain growth and contraction, for the same initial and final domain size, γ_0. Activator $v(x,t)$ profiles are plotted for (a) increasing and (b) decreasing domain size (γ). The domain grows until time $t' = 2500$ from which point the domain is contracting. In the simulation we take $\rho = 0.001$ for $\gamma(t)$ given by equation (4.48) with $\gamma_0 = 1$, with Schnakenberg kinetics and $d = 0.05$.

4.6 Discussion

The slow growth limit that we have considered in this chapter seems reasonable in the context of biological pattern formation. When the spatial domain is changing length on a timescale which is commensurable with the time taken for pattern formation there is no quasi-steady behaviour, and the resulting evolving spatial profile appears to be quite disorganised. We have seen that the pattern sequence may depend on the rate and functional form of the change in γ with time. This indicates that the solution does not adiabatically follow steady solution branches during transitions between patterns. The dynamics which take the evolving spatial profile from the vicinity of one bifurcation branch to another is investigated in the following chapter. Under slow growth a dilution term appears which slightly modifies the kinetics. This term has a magnitude which is on the order of the slow rate of change of the domain size. In fact the symmetry argument and the conclusions that have been drawn are equally valid if this modification to the kinetics is neglected.

The symmetry analysis that allowed us to predict FD for exponential domain growth and conditions on the growth rate parameter ρ for linear domain growth reflects the symmetry in the underlying solutions to the steady state problem. Similar arguments have been proposed recently by Nishiura and Ueyama [95] for the bistable Gray-Scott model, to explain the closely related phenomenon of self-replicating patterns on the fixed domain. Numerically it is found that a pattern initiated in some region of a domain spreads to fill the domain by splitting of the outermost peaks (see Figure 2.7(b)). The authors suggest that the symmetry in the steady state equations that we have demonstrated in Chapter 2, which they call 'folding-up', causes related inhomogeneous solution branches to line up in the bifurcation diagram, so that the saddle-node bifurcation points at which they are created line up at the same value of the control parameter. The authors call this the 'edge of hierarchy structure of limiting points'. The trajectory of the PDE solution from suitably chosen initial data passes close to each of these limiting points of the branches so that transient patterns approximating the steady solutions are observed for the full PDE system. In the present work the situation is somewhat different in that we have a time dependent γ, which may be thought of as the control parameter. However, it seems that the symmetry identified in the steady state problem may be responsible for both results. Furthermore, we have been able to show that in our model the symmetry argument can be extended into the full PDE system.

Linear analysis identifies a minimum domain length (and hence a minimum γ) for each pattern mode. The critical domain length for solutions corresponding to patterns of the lowest mode (the half- or boundary-peak) gives a minimum domain length below which no Turing bifurcation is possible (however, for subcritical bifurcation, inhomogeneous solution branches may exist below this point). For the numerical computations in this chapter the initial domain length has been taken to be smaller

than the critical domain length. As the domain grows the first destabilising mode, the lowest admissible pattern, is excited as the domain length increases through the critical point ($\gamma = \gamma_c$). However, if the initial domain is sufficiently large that patterns of higher mode may be excited, then the FD sequence which ensues may be based on a different initial mode. In general, if the initial mode to be excited through the Turing bifurcation is mode $m = m_0$ then the sequence will comprise modes $m_0 \times 2^n$. However, we reiterate that pattern selection becomes increasingly unreliable as the domain length increases, and close control of initial data and domain length is required to select initial patterns of large mode number m_0. For this reason the mechanism that we have described in this chapter for uniform domain growth is not well suited to reliably generating patterns with an odd number of peaks, which require higher m_0. We will reconsider this later in the context of nonuniform domain growth.

We have demonstrated that a reaction-diffusion mechanism on a growing one-dimensional domain can reliably generate patterns with multiple periodic peaks. This is contrary to the conclusions of Saunders and Ho [118] which are based on the numerical simulations of the model by Arcuri and Murray [3] (AM). Here the authors nondimensionalise time using T_D, the diffusive relaxation time (see (2.6), by writing $\bar{t} = \omega t/\gamma$ and subsequently impose time dependence on γ where it appears explicitly in the evolution equation (3.1). The timescales for pattern formation and for domain growth, the importance of which we have emphasised, thus become conflated. This distorts the evolution of pattern sequences in the AM model, which fails to produce the robust sequences we have found. Neglecting the dilution term, one may transform the AM equations into our model by defining a new time variable $z = \int_0^t \mathrm{d}t/\gamma(t)$. The time dependence for γ in the AM equations which corresponds to an exponentially growing domain may then be found, namely $\gamma(z) = \gamma_0/(1 - 2\rho\gamma_0 z)$. Numerical solutions of equation (3.1) with this form for $\gamma(z)$ show that FD behaviour is observed in the AM model with the appropriate time dependence, for $z < 1/2\rho\gamma_0$ where $\gamma(z)$ becomes singular.

The strong tendency to splitting of activator peaks (and insertion for the Gierer-Meinhardt kinetics) is striking. Following breakdown of the FD sequence for linear growth, subsequent patterns still develop by splitting (for Schnakenberg kinetics) of a subset of the peaks on the domain, to give activator patterns with internalised peaks. In the following chapter we examine this tendency for splitting and insertion of new peaks in more detail.